Power Beacon and NOMA-Assisted Cooperative IoT Networks With Co-Channel Interference: Performance Analysis and Deep Learning Evaluation

Anh-Tu Le, *Member, IEEE*, Dinh-Hieu Tran, *Student Member, IEEE*, Chi-Bao Le, Phu Tran Tin, Tan N. Nguyen, *Member, IEEE*, Zhiguo Ding, *Fellow, IEEE*, H. Vincent Poor, *Life Fellow, IEEE*, and Miroslav Voznak, *Senior Member, IEEE*

***Abstract*—This study investigates a two-way relaying non-orthogonal multiple access (TWR-NOMA) enabled Internet-of-Things (IoT) network, in which two NOMA users communicate via an IoT access point (IAP) relay using a decode-and-forward (DF) protocol. A power beacon (PB) is used to power the IAP to address the IAP's limited lifetime due to energy constraints. Since co-channel interference (CCI) is inevitable in IoT systems, this effect is also studied in the proposed system to improve practicality. Based on the proposed system model, the closed-form equations for the exact and asymptotic outage probability (OP) and ergodic data (ED) of the NOMA users' signals are first derived to describe the performance of TWR-NOMA systems. The system's diversity order and throughput are then evaluated according to the derived results. To further improve the system's performance, a low-complexity strategy 2D golden section search (GSS) is performed, subject to power allocation (PA) and time-switching (TS) factors, to optimize the outage performance. Finally, a deep learning design with minimal computing complexity and precision OP prediction is established for a real-time IoT network configuration. The numerical results are discussed and analyzed in terms of the effects of the CCI, the TS ratio, the PA factor, the fading parameter on the OP, system throughput, and ED.**

***Index Terms*—Co-channel interference, deep neural network, energy harvesting, Internet of Things, non-orthogonal multiple access, power beacon, two-way relay, wireless power transfer.**

I. Introduction

The Internet of Things (IoT) is an emerging technology that has been heavily studied by both academia and industry and promises solutions for improving quality of life. Specifically, the IoT is able to connect devices that collect data in systems designed for intelligent transportation, smart cities, environmental/disaster/agricultural monitoring, health care, and many other relevant areas [1], [2], [3], [4]. However, the range of IoT applications requires widespread adoption of inexpensive, battery-operated devices with differing quality-of-service (QoS) standards. Battery longevity is important because the maintenance can be difficult or impossible to perform for large-scale or challenging deployments [5]. In recent years, energy harvesting (EH) technology has been studied as a promising solution for prolonging the lifespans of IoT devices. Besides using ambient sources such as solar [6], wind, geothermal, electromagnetic and vibrational energy [7], [8], wireless power transfer (WPT) is a potentially useful technology for its predictability and management capabilities [9], [10], [11], [12], [13]. Radio frequency (RF) WPT, in which IoT users gather RF energy and convert it into electricity, can power IoT networks at distances of more than 6 km [14], [15]. WPT can be classified into two types: wireless-powered communication networks (WPCNs) and simultaneous wireless information and power transfer (SWIPT) [16], [17], [18], [19], [20]. Both SWIPT and WPCN can be used with IoT devices (IoTDs), but systems employing SWIPT are more suitable for short-distance communications [21] while WPCN functions better with long-distance communications by deploying power stations, otherwise known as power beacons (PBs), to recharge IoTDs through RF signals [22].

Motivated by the advantages of PBs for longer-distance charging in wireless, a number of studies have investigated the features

Manuscript received 29 May 2023; revised 16 October 2023; accepted 9 November 2023. Date of publication 17 November 2023; date of current version 7 May 2024. This work was supported in part by the European Union within the REFRESH project - Research Excellence For Region Sustainability and High-tech Industries ID under Grant CZ.10.03.01/00/22_003/0000048 of the European Just Transition Fund, in part by the Ministry of Education, Youth and Sports of the Czech Republic (MEYS CZ) through the project SGS ID under Grant SP 7/2023 conducted by VSB - Technical University of Ostrava, and in part by the U.S National Science Foundation under Grants CNS-2128448 and ECCS-2335876 for H. Vincent Poor. Recommended for acceptance by T. Shu. *(Corresponding author: Tan N. Nguyen.)*

Anh-Tu Le and Miroslav Voznak are with the Faculty of Electrical Engineering and Computer Science, VSB - Technical University of Ostrava, 70800 Ostrava, Czech Republic (e-mail: tu.le.anh.st@vsb.cz; miroslav.voznak@vsb.cz).

Dinh-Hieu Tran was with the Interdisciplinary centre for Security Reliability and Trust (SnT), University of Luxembourg, 4365 Esch-sur-Alzette, Luxembourg. He is now with Nokia Bell Labs, 91300 Massy, France (e-mail: dinh-hieu.tran@nokia.com).

Chi-Bao Le is with Transcosmos Vietnam, Ho Chi Minh City 700000, Vietnam (e-mail: bao.lc@trans-cosmos.com.vn).

Phu Tran Tin is with the Data Science Laboratory, Faculty of Information Technology, Ton Duc Thang University, Ho Chi Minh City, Vietnam (e-mail: phutrantin@tdtu.edu.vn).

Tan N. Nguyen is with the Communication and Signal Processing Research Group, Faculty of Electrical and Electronics Engineering, Ton Duc Thang University, Ho Chi Minh City 70000, Vietnam (e-mail: nguyennhattan@tdtu.edu.vn).

Zhiguo Ding is with the Electrical and Computer Engineering (ECE), Department at Khalifa University, Abu Dhabi, UAE (e-mail: zhiguo.ding@ieee.org).

H. Vincent Poor is with the Department of Electrical and Computer Engineering, Princeton University, Princeton, NJ 08544 USA (e-mail: poor@princeton.edu).

This article has supplementary downloadable material available at https://doi.org/10.1109/TMC.2023.3333764, provided by the authors.

Digital Object Identifier 10.1109/TMC.2023.3333764

and applications of PB with WPCN in different contexts [23], [24], [25]. Nikoletseas et al. [23] proposed a scenario in which PB transfers power to rechargeable devices despite certain technological limitations. Specifically, the authors attempted to increase the transferable energy while limiting the maximum level of the RF signals to eliminate any potential harm to human health. Dai et al. [24] applied a similar strategy, using the super-distribution characteristics of the received power per sensor to maximize the charging utility function of EH while limiting the RF electromagnetic field level mode. Hieu et al. [25] studied the performance of multi-hop multi-path wireless sensor networks (WSNs) and the effects of hardware impairments (HI) and eavesdroppers on these networks. Specifically, IoTDs can be used to harness energy from a PB for data transmission.

Non-orthogonal multiple access (NOMA) has been developed as one of the key technologies in beyond 5G/6G since it can help support massive connectivity at relatively low cost, and increase spectral efficiency (SE) by enabling multiple IoTDs to access the same wireless resources (e.g., time, frequency, spreading code) [26], [27], [28], [29]. In principle, NOMA multiplexes multiple signals or messages for different IoTDs with different channel conditions via the power or code domain to create a balanced trade-off between user fairness and system performance [26]. For example, in power-domain NOMA (PDNOMA), when a low-power IoTD obtains a NOMA signal in strong channel conditions, it first decodes the user symbol with higher power as if worse channel conditions existed and then subtracts its partner's signal to decode its own symbol. On the other hand, a high-power IoTD decodes its signal by treating the lower-power IoTD's signal as noise. Via this mechanism, commonly referred to as successive interference cancellation (SIC), IoTD signals can be separated by the receivers. In this way, NOMA can achieve significant improvements in SE and system capacity (SC) compared to orthogonal multiple access (OMA) approaches [30], [31], [32], [33].

Despite exhibiting many advantages, all the above-mentioned studies consider only one-way relaying networks (OWRNs). Recent studies have introduced two-way relaying networks (TWRNs), which can improve SE over OWRN [34], [35]. The underlying concept of a TWRN is to transmit information between two nodes via a relay, possibly using either an amplify-and-forward (AF) or a decode-and-forward (DF) protocol [36], [37], [38]. Jang et al. [36] investigated the performance of multi-user (MU) TWRN channels for half-duplex (HD) AF relays, focusing on user selection. Zheng et al. [37] combined rate splitting and user grouping protocols for multi-pair TWR-NOMA networks to improve resource management and increase throughput. Lv et. al [38] developed a joint antenna and relay selection scheme to improve transmission reliability for multiple access and time division broadcast relaying techniques in TWR-NOMA-based networks optimized for transmitting power allocation.

Deep learning is a powerful, data-driven method for resolving a range of challenges such as image processing, pattern recognition, and wireless communications applications [39]. Zhang et al. [40] developed a deep neural network (DNN) for regression and classification problems in the cognitive two-way relaying network for selection. Wang [41] studied two-hop wireless networks and machine learning-based relay selection and transformed best relay selection (BRS) into a multi-class classification problem by using a decision-tree-based selection method. Tseng et al. [42] performed grouping/subcarrier assignment tasks based on a DNN and supervised learning for multilayer resource allocation in NOMA video communications systems. The authors [43] also enhanced their method of accounting for outage capacity and maximizing ergodic capacity to produce ultra-reliable low-latency communications (URLLC) 5G system. Ye et al. [44], however, proposed a specifically generated DNN to enhance the dependability gain achieved by a grant-free NOMA system.

A. *Motivations and Contribution*

For additional improvements in the energy efficiency (EE) and SE of TWR networks, the current study explores a TWR that cooperates with NOMA and is aided by a PB under co-channel interference (CCI). Recent works have also investigated TWR-NOMA systems [45], [46], [47], Khalid and Jangsher [45] analyzed an upper bound on the capacity of a TWR system used in connection with a multi-user multiple-input multiple-output (MU-MIMO) NOMA system. Zheng et al. [46] studied a secure NOMA-based bidirectional relay network with full-duplex forwarding. Yue et al. [47] derived closed-form expressions for outage probability (OP) in TWR-NOMA with both perfect and imperfect SIC. However, the authors did not consider PB in TWR-NOMA to improve energy sustainability. In addition, DNN techniques have lately emerged as a potent tool for network performance evaluation [48], [49], [50], using the benefit of data-driven approaches to solve the computationally infeasible or unnecessarily complicated tasks of a traditional model-based approach. Thus, the problem of identifying outage performance may be solved by taking advantage of the advantages of DNN approaches. The current study investigates an effective DNN-based strategy to develop an in-depth model that reduces total energy consumption through an offline training process. We show that this DNN-based approach for power beacon-assisted TWR-NOMA networks in the presence of CCI offers excellent advantages. In particular, our contributions are as follows:

- A proposed PB-assisted two-way NOMA IoT system in the presence of CCI, in which an IoT access point (IAP) harvests energy from a PB using a time-switching (TS) EH method to overcome its limited energy constraint. The IAP then uses harvested energy to exchange information with two IoT users to attain a battery-free IoT system.
- Exact closed-form expressions for the OP, ED and asymptotic OP. The throughput of the proposed system is also addressed. Two algorithms for determining the optimal PA coefficient and EH times for two IoT users are proposed, which further improve the proposed IoT NOMA system's performance.
- A low-complexity strategic 2D gold section search (GSS) is performed to find the optimal power allocation (PA) and the optimal EH time coefficient in order to minimize the outage probability.

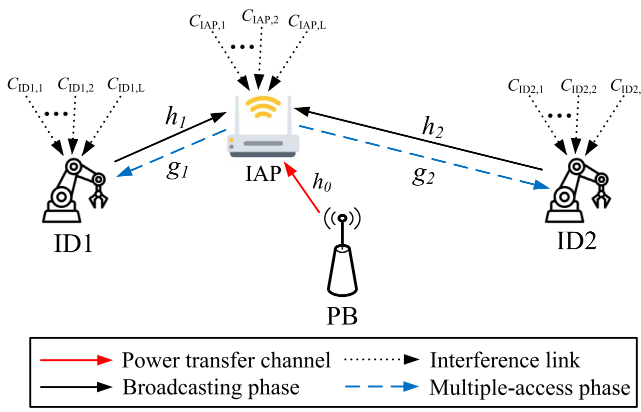

Fig. 1. System model of a two-way relay EH-NOMA.

- A DNN model designed to predict the OP and throughput of the proposed TWR-NOMA IoT system. In the context of a complicated network, It is demonstrated that, in complex network contexts, the DNN models are effective in predicting performance using a low-latency inference process.
- Comprehensive, real-world information about how various system factors affect overall network performance. The study also shows that the outcomes of the simulation exactly match the results of the derivation analysis and establish the accuracy of its analytical derivations. The proposed DNN model also exhibits low computational expenditure and fast execution time; it can predict OP and obtain throughput results which closely approximate the results obtained from analytical and simulation methods.

B. Organization

The paper is organized as follows: Section II describes the proposed system model; Section III analyzes the exact and asymptotic outage probabilities, system throughput and diversity order; Section IV discusses an evaluation of the DNN; Section V presents and discusses the numerical results; finally, Section VI summarizes the paper's contributions.

II. System Model and Channel Characteristics

A. System Description

Fig. 1 illustrates the scheme of a TWR-NOMA-enabled IoT network with PB support, in which an IAP equipped with a single antenna collects energy from a PB and serves two IoT users[1] (a near user ID1 and far user ID2) in HD mode. The IAP must draw energy from a PB because its own available energy is limited; the PB acts as a power source to maintain the IAP's operation and is positioned in a suitable place to enable the PB-IAP link. As in the study by Wang et al. [52], the current study assumes no direct connection between the two IoT users due to the significant shadowing effects caused by physical barriers. Aided by a specific IAP, communication between the two users is enabled, and perfect channel state information (CSI) is assumed to be at each receiver. This type of system can also be applied in other IoT systems, for example, smart home appliances, RFID logistics, security monitoring, and warehouse management. The CCI generated by multiple signals, however, may impact a network and impair a system's overall performance, but it can also be exploited as an extra energy source to facilitate IAP to IoT user transmission by the IAP's harvesting mechanism. The current study assumes that fading channels follow a Nakagami-m distribution; as commonly made in the literature [53], CCI also follows a Nakagami-m distribution.[2] Furthermore, the detail of the parameter definition can be listed in Table I.

TABLE I
Parameter Definitions

Parameter	Definition
x_{ID1}, x_{ID2}	Transmission signals to ID1 and ID2
$x_{\mathrm{IAP},l}$, $x_{\mathrm{IDi},l}$	Transmit information of l^{th} interference
ω_{IAP}, ω_{IDi}	Additive White Gaussian noise
P_U	Total transmission power of two users
P_I	Transmitted power from interference
P_0	Transmitted power from IAP
a_i	Corresponding power allocation coefficient
η	Energy conversion efficiency
α	Time allocation parameter
L	Co-channel interference
N_0	Noise variance
R_i	Target Rate in bps/Hz.
h_0	Channel gain from PB to IAP
h_1	Channel gain from ID1 to IAP
h_2	Channel gain from ID2 to IAP
g_1	Channel gain from IAP to ID1
g_2	Channel gain from IAP to ID2

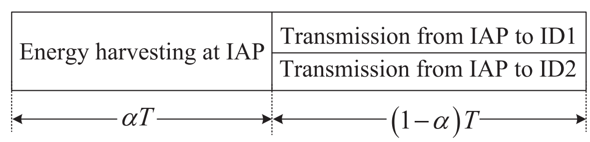

Fig. 2. Scheme of the TS protocol.

1) Energy Harvesting and Data Transmission in the First Phase: The IAP harvests energy from the PB according to a TS relaying protocol, as depicted in Fig. 2. We assume that T is the total communications time for transmitting data from the IAP to the two devices. During the initial αT time $(0 < \alpha < 1)$, the IAP harvests energy from the PB. The remaining $(1 - \alpha)T$ time is divided equally between data transmissions at the IAP.

In the energy harvesting phase, the energy harvested by the IAP in the period αT is given by

$$E_{\mathrm{IAP}} = T\alpha\eta P_0|h_0|^2, \tag{1}$$

where η is the energy conversion efficiency of energy harvesting circuit $(0 < \eta < 1)$, P_0 denotes the transmitting power of the PB, and h_0 is the channel power gain of the link from the PB to the IAP.

[1] IoT users include sensors, camera controls and public smart devices such as traffic lights and LED advertising panels, etc. [51]

[2] Nakagami-m is a generic form which can describe both Rayleigh and Rician distributions. Details are discussed in Section [3.2.2] in [54].

Referring to the study in [55], the transmitting power of the IAP is expressed as

$$P_{\mathrm{IAP}} = \frac{E_{\mathrm{IAP}}}{(1-\alpha)\,T} = \alpha\eta P_0 (1-\alpha)^{-1} |h_0|^2. \tag{2}$$

When the two users transmit their signals to the IAP, the baseband signal y_{IAP}, is given by

$$y_{\mathrm{IAP}} = \underbrace{\sqrt{a_1 P_U} h_1 x_{\mathrm{ID1}} + \sqrt{a_2 P_U} h_2 x_{\mathrm{ID2}}}_{\text{Desired Signal}} + \underbrace{\sum_{l=1}^{L} \sqrt{P_{I_l}} c_{\mathrm{IAP},l} x_{\mathrm{IAP},l}}_{\text{Interference}} + \underbrace{\omega_{\mathrm{IAP}}}_{\text{Noise}}, \tag{3}$$

where a_1 and a_2 are the NOMA allocation coefficients satisfying the conditions $a_1 > a_2$ and $a_1 + a_2 = 1$, h_1 and h_2 represent the respective channel coefficients from ID1 and ID2 to the IAP, P_U denotes the total transmission power of the two users, and x_{ID1} and x_{ID2} are the respective signals from ID1 and ID2. The signals are assumed to have unit power, i.e., $\mathbb{E}\{|x_{\mathrm{ID1}}|^2\} = \mathbb{E}\{|x_{\mathrm{ID2}}|^2\} = 1$. P_{I_l} is the transmitting power of the lth interference source, $c_{\mathrm{IAP,l}}$ is the channel coefficient between the IAP and its lth interference, $x_{\mathrm{IAP},l}$ denotes the signal of lth interference at the IAP, where $\mathbb{E}\{|x_{\mathrm{IAP},l}|^2\} = 1$, and $\omega_{\mathrm{IAP}} \sim \mathcal{CN}(0, N_0)$ is the additive white Gaussian noise (AWGN). It should be noted that effective uplink power control can improve the performance of these systems; however, this is beyond the scope of this paper.

The proximity of ID1 to the IAP gives it priority to decode its own signal first. The received signal-to-interference plus noise ratio (SINR) for the relay to decode the signal x_{ID1} is expressed as

$$\begin{aligned}\gamma_{\mathrm{IAP}}^{x_{\mathrm{ID1}}} &= \frac{a_1 P_U |h_1|^2}{a_2 P_U |h_2|^2 + \sum_{l=1}^{L} |P_{I_l} c_{\mathrm{IAP},l}|^2 + N_0} \\ &= \frac{a_1 \rho_S |h_1|^2}{a_2 \rho_S |h_2|^2 + \rho_I \gamma_{\mathrm{I,IAP}} + 1},\end{aligned} \tag{4}$$

where $\gamma_{\mathrm{I,IAP}} = \sum_{l=1}^{L} |c_{\mathrm{IAP},l}|^2$, with the assumption that $P_I = P_{I_l}, \forall l$, and $P_0 = P_U$, thus $\rho_I = P_I/N_0$ and $\rho_S = P_U/N_0 = P_0/N_0$.

Under the condition that the IAP correctly interprets the signal from ID1. The received SINR for the IAP to decode the signal x_{ID2} once the SIC has removed signal x_{ID1} from (4) is stated as

$$\gamma_{\mathrm{IAP}}^{x_{\mathrm{ID2}}} = \frac{a_2 \rho_S |h_2|^2}{\rho_I \gamma_{\mathrm{I,IAP}} + 1}. \tag{5}$$

2) Downlink NOMA Process in the Second Phase: In the second phase, the signal received at IDi, where $i \in \{1, 2\}$, is given by

$$y_{\mathrm{ID}i} = \underbrace{g_i \left(\sqrt{b_1 P_{\mathrm{IAP}}} x_{\mathrm{ID1}} + \sqrt{b_2 P_{\mathrm{IAP}}} x_{\mathrm{ID2}}\right)}_{\text{Desired Signal}} + \underbrace{\sum_{l=1}^{L} \sqrt{P_{I_l}} c_{\mathrm{ID}i,l} x_{\mathrm{ID}i,l}}_{\text{Interference}} + \underbrace{\omega_{\mathrm{ID}i}}_{\text{Noise}}, \tag{6}$$

where $b_1 = 1 - a_1, b_2 = 1 - a_2, P_{\mathrm{IAP}}$ denotes the transmission power at the IAP, g_1 and g_2 represent the respective channel coefficients from the IAP to ID1 and ID2, and $\omega_{\mathrm{ID}i} \sim \mathcal{CN}(0, N_0)$ denotes the AWGN with zero-mean and variance N_0. In addition, $c_{\mathrm{ID}i,l}$ is the channel coefficient between USi and its lth interference, and $x_{\mathrm{ID}i,l}$ denotes the signal of lth interference at the two users, where $\mathbb{E}\{|x_{\mathrm{ID}i,l}|^2\} = 1$.

From (6), since the NOMA scheme is adopted, ID1 first decodes the information intended for ID2, x_{ID2}, by treating x_{ID1} as the noise. Hence, the SINR received at the ID1 to detect x_{ID2} is given by

$$\gamma_{\mathrm{ID1}}^{x_{\mathrm{ID2}}} = \frac{b_2 P_{\mathrm{IAP}} |g_1|^2}{b_1 P_{\mathrm{IAP}} |g_1|^2 + \sum_{l=1}^{L} |P_{I_l} c_{\mathrm{ID1},l}|^2 + N_0}. \tag{7}$$

By substituting P_{IAP} in (2) into (7), we rewrite

$$\gamma_{\mathrm{ID1}}^{x_{\mathrm{ID2}}} = \frac{b_2 \theta |h_0|^2 |g_1|^2}{b_1 \theta |h_0|^2 |g_1|^2 + \rho_I \gamma_{\mathrm{I,ID1}} + 1}, \tag{8}$$

where $\gamma_{\mathrm{I,ID1}} = \sum_{l=1}^{L} |c_{\mathrm{ID1},l}|^2$ and $\theta = \frac{\alpha\eta\rho_S}{(1-\alpha)}$.

By assuming perfect SIC for NOMA, the SINR at ID1 to detect x_{ID1} are therefore expressed as

$$\gamma_{\mathrm{ID1}}^{x_{\mathrm{ID1}}} = \frac{b_1 \theta |h_0|^2 |g_1|^2}{\rho_I \gamma_{\mathrm{I,ID1}} + 1}. \tag{9}$$

Finally, ID2 detects its own signal x_{ID2}, treating x_{ID1} as noise. The instantaneous SINR at ID2 from (6) is written as

$$\gamma_{\mathrm{ID2}}^{x_{\mathrm{ID2}}} = \frac{b_2 \theta |h_0|^2 |g_2|^2}{b_1 \theta |h_0|^2 |g_2|^2 + \rho_I \gamma_{\mathrm{I,ID2}} + 1}, \tag{10}$$

where $\gamma_{\mathrm{I,ID2}} = \sum_{l=1}^{L} |c_{\mathrm{ID2},l}|^2$.

B. Channel Characteristics

Let $Z \in \{h_0, h_i, g_i\}$ and $i \in \{1, 2\}$; the probability density function (PDF) and cumulative distribution function (CDF) of Z are given by [56]

$$f_{|Z|^2}(x) = \frac{x^{m_Z - 1}}{\Gamma(m_Z)\,\lambda_Z^{m_Z}} e^{-\frac{x}{\lambda_Z}}, \tag{11}$$

and

$$\begin{aligned}F_{|Z|^2}(x) &= \frac{1}{\Gamma(m_Z)} \gamma\left(m_Z, \frac{x}{\lambda_Z}\right) \\ &= 1 - e^{-\frac{x}{\lambda_Z}} \sum_{s=0}^{m_Z - 1} \frac{x^s}{s!\lambda_Z^s},\end{aligned} \tag{12}$$

where $\lambda_Z = \frac{\Omega_Z}{m_Z}$, m_Z is the fading severity parameter, $\Omega_Z = \mathbb{E}[|Z|^2]$ is the average power, $\Gamma(x) = (x-1)!$ is the Gamma function and $\gamma(.,.)$ is the lower incomplete Gamma function.

Lemma 1: The corresponding PDF and CDF of the cascaded channel gains h_0 and g_i are $f_{|h_0|^2|g_i|^2}(x)$ and $F_{|h_0|^2|g_i|^2}(x)$, expressed by

$$f_{|h_0|^2|g_i|^2}(x) = \frac{2x^{\frac{m_{g_i}+m_{h_0}}{2}-1} K_{m_{h_0}-m_{g_i}}\left(2\sqrt{\frac{x}{\lambda_{g_i}\lambda_{h_0}}}\right)}{\Gamma(m_{h_0})\Gamma(m_{g_i})\left(\sqrt{\lambda_{h_0}\lambda_{g_i}}\right)^{m_{h_0}+m_{g_i}}}, \tag{13}$$

and

$$F_{|h_0|^2|g_i|^2}(x) = 1 - \sum_{a=0}^{m_{h_0}-1} \frac{2}{\Gamma(m_{g_i})\, a!} \times \left(\sqrt{\frac{x}{\lambda_{h_0}\lambda_{g_i}}}\right)^{m_{g_i}+a} K_{m_{g_i}-a}\left(2\sqrt{\frac{x}{\lambda_{h_0}\lambda_{g_i}}}\right), \tag{14}$$

where $K_a(.)$ is the modified Bessel function of the second kind and a order.

Proof: The term PDF $f_{|h_0|^2|g_i|^2}(x)$ can be calculated as

$$f_{|h_0|^2|g_i|^2}(x) = \int_0^\infty \frac{1}{y} f_{|h_0|^2}(y) f_{|g_i|^2}\left(\frac{x}{y}\right) dy. \tag{15}$$

By applying (11), the PDF can be rewritten as

$$f_{|h_0|^2|g_i|^2}(x) = \frac{x^{m_{g_i}-1}}{\Gamma(m_{h_0})\lambda_{h_0}^{m_{h_0}}\Gamma(m_{g_i})\lambda_{g_i}^{m_{g_i}}} \times \int_0^\infty y^{m_{h_0}-m_{g_i}-1} e^{-\frac{m_{h_0}}{\lambda_{h_0}}y} e^{-\frac{m_{g_i}x}{\lambda_{g_i}y}} dy. \tag{16}$$

Based on [57, Eq. (3.471.9)], $f_{|h_0|^2|g_i|^2}(x)$ can be formulated as

$$f_{|h_0|^2|g_i|^2}(x) = \frac{2x^{\frac{m_{g_i}+m_{h_0}}{2}-1} K_{m_{h_0}-m_{g_i}}\left(2\sqrt{\frac{x}{\lambda_{g_i}\lambda_{h_0}}}\right)}{\Gamma(m_{h_0})\Gamma(m_{g_i})\left(\sqrt{\lambda_{h_0}\lambda_{g_i}}\right)^{m_{h_0}+m_{g_i}}}. \tag{17}$$

Furthermore, the term CDF $F_{|h_0|^2|g_i|^2}(x)$ is calculated as

$$F_{|h_0|^2|g_i|^2}(x) = \Pr\left(|h_0|^2 < \frac{x}{|g_i|^2}\right) = \int_0^\infty F_{|h_0|^2}\left(\frac{x}{y}\right) f_{|g_i|^2}(y) dy. \tag{18}$$

Using (11), (12) and [57, Eq. (8.352)], we obtain

$$F_{|h_0|^2|g_i|^2}(x) = 1 - \sum_{a=0}^{m_{h_0}-1} \frac{1}{\Gamma(m_{g_i})\lambda_{g_i}^{m_{g_i}} a!}\left(\frac{x}{\lambda_{h_0}}\right)^a \times \int_0^\infty y^{m_{g_i}-a-1} e^{-\frac{x}{y\lambda_{h_0}}-\frac{y}{\lambda_{g_i}}} dy. \tag{19}$$

Similarly, the term CDF $F_{|h_0|^2|g_i|^2}(x)$ is given by

$$F_{|h_0|^2|g_i|^2}(x) = 1 - \sum_{a=0}^{m_{h_0}-1} \frac{2}{\Gamma(m_{g_i})\, a!} \times \left(\sqrt{\frac{x}{\lambda_{h_0}\lambda_{g_i}}}\right)^{m_{g_i}+a} K_{m_{g_i}-a}\left(2\sqrt{\frac{x}{\lambda_{h_0}\lambda_{g_i}}}\right). \tag{20}$$

The proof is complete. ∎

In addition, where $b \in \{\text{IAP}, \text{ID1}, \text{ID2}\}$, $|c_{b,l}|^2$ follows a Gamma distribution with a fading severity parameter $m_{b,l}$ and average power $\Omega_{b,l}$. Next, we assume that $m_b = m_{b,l}$, $\Omega_b = \Omega_{b,l}$, $\forall i$. Furthermore, $\gamma_{I,b}$ follows the sum of the Gamma distribution. Therefore, the PDF and CDF of $\gamma_{I,b}$ are respectively given by

$$f_{\gamma_{I,b}}(x) = \frac{x^{Lm_b-1}}{\Gamma(Lm_b)\lambda_b^{Lm_b}} e^{-\frac{x}{\lambda_b}}, \tag{21}$$

and

$$F_{\gamma_{L,b}}(x) = \frac{1}{\Gamma(Lm_b)}\gamma\left(Lm_b, \frac{x}{\lambda_b}\right) = 1 - e^{-\frac{x}{\lambda_b}} \sum_{t=0}^{Lm_b-1} \frac{x^t}{t!\lambda_b^t}. \tag{22}$$

III. Performance Analysis

In this section, the analytical equations for the system are derived, taking into account the outage probability. Diversity ordering and asymptotic outage behavior are also discussed, and the system throughput is then determined.

A. Outage Probability Analysis

The performance of TWR-NOMA is characterized in terms of outage probability. The following section details the outage probabilities due to the channel reciprocity of ID1 and ID2.

1) Outage Probability of ID1*:* In a TWR-NOMA system, ID1 outage events are characterized by: (i) IAP cannot correctly decode x_{ID1}; (ii) ID1 cannot detect the information x_{ID2}; (iii) ID1 cannot detect x_{ID2}, but can successfully decode x_{ID1}. For the purposes of streamlining the current study, the complementary events of x_{ID1} represent the outage probability. Consequently, the outage probability at ID1 for a TWR-NOMA system is expressed as

$$\mathcal{P}_{\text{ID1}} = 1 - \Pr\left(\gamma_{\text{IAP}}^{x_{\text{ID1}}} > \varepsilon_1, \gamma_{\text{ID1}}^{x_{\text{ID2}}} > \varepsilon_2, \gamma_{\text{ID1}}^{x_{\text{ID1}}} > \varepsilon_1\right), \tag{23}$$

where $\varepsilon_i = 2^{\frac{R_i}{1-\alpha}} - 1$, with R_i being the target rate at of IDi.

Proposition 1: A closed-form expression for the outage probability at ID1 for TWR-NOMA is given by (24), shown at the bottom of the next page, where $\zeta_1 = \frac{\varepsilon_1}{a_1\rho_S}$, $\xi_{\max} = \max(\xi_2, \xi_1)$, $\xi_1 = \frac{\varepsilon_1}{a_1\theta}$, $\xi_2 = \frac{\varepsilon_2}{\theta(a_2-\varepsilon_2 a_1)}$, $\Theta = \sqrt{\frac{\xi_{\max}}{\lambda_{h_0}\lambda_{g_1}}}$, $\psi = \frac{1}{\Gamma(m_{h_2})\Gamma(Lm_{\text{IAP}})\lambda_{\text{IAP}}^{Lm_{\text{IAP}}}\lambda_{h_2}^{m_{h_2}}}$, $\delta_1 = (\frac{1}{\lambda_{h_2}} + \frac{a_2\rho_S\zeta_1}{\lambda_{h_1}})$, $\delta_2 = (\frac{1}{\lambda_{\text{IAP}}} + \frac{\rho_I\zeta_1}{\lambda_{h_1}})$, $\phi_1 = (-1)^{Lm_{\text{ID1}}-r-1}\Theta^{m_{g_1}+c}$, and $H_{p,q:u,v:e,f}^{n,m:s,t:i,j}(.)$ is the extended generalized bivariate Fox's H-function (EGBFHF)[3] as defined in [60, Eq. (2.57)].

Proof: See Appendix A, available online.

2) Outage Probability of ID2: The following scenarios describe additional outage events at ID2 for NOMA. One scenario is that the IAP might first detect x_{ID2} by decoding information

[3]Both MATLAB and MATHEMATICA implementations of the EGBFHF are described in [58] and [59].

x_{ID1}, then x_{ID2}. Another case is when ID2 can reliably find x_{ID2}. The outage probability of ID2 can therefore be written as

$$\mathcal{P}_{\mathrm{ID2}} = 1 - \Pr\left(\gamma_{\mathrm{IAP}}^{x_{\mathrm{ID1}}} > \varepsilon_1, \gamma_{\mathrm{IAP}}^{x_{\mathrm{ID2}}} > \varepsilon_2, \gamma_{\mathrm{ID2}}^{x_2} > \varepsilon_2\right). \quad (25)$$

Proposition 2: A closed-form expression for the outage probability of ID2 is given by (26), shown at bottom of this page, where $\Xi = \sqrt{\frac{\xi_2}{\lambda_{h_0}\lambda_{g_2}}}$, $\phi_2 = (-1)^{Lm_{\mathrm{ID2}}-r-1}\Xi^{m_{g_2}+c}$ and $\zeta_2 = \frac{\varepsilon_2}{a_2\rho_S}$.

Proof: See Appendix B, available online.

B. Asymptotic Computation of the Main Performance Metric

To gain more insight into the high power regime, this section examines the asymptotic expressions for the main performance metric.

Considering the analytical findings in (35) and (51), when $\rho_S \to \infty$, the asymptotic expression for $\mathcal{P}^{\infty} = \mathcal{P}_{\mathrm{ID1}}^{\infty} = \mathcal{P}_{\mathrm{ID2}}^{\infty}$, with $A_1^{\infty} = A_3^{\infty} = \Pr(\frac{a_1|h_1|^2}{a_2|h_2|^2} > \varepsilon_1)$ and $A_2^{\infty} = A_4^{\infty} = 1$, is written as

$$\mathcal{P}^{\infty} = 1 - \sum_{s=0}^{m_{h_1}-1} \frac{\Gamma(m_{h_2}+s)\,\varepsilon_1^s a_2^s a_1^{m_{h_2}} \lambda_{h_1}^{m_{h_2}} \lambda_{h_2}^s}{s!\Gamma(m_{h_2})(a_1\lambda_{h_1} + \lambda_{h_2}\varepsilon_1 a_2)^{m_{h_2}+s}}. \quad (27)$$

Remark 1: From the definition of the diversity order, which is defined as [61] $\bar{d} = -\lim_{\rho_S\to\infty} \frac{\log(\mathcal{P}^{\infty})}{\log(\rho_S)}$ when ρ_S approaches infinity, a diversity order of 0 is achieved. Under the NOMA protocol, a user experiences interference from other signals because it first decodes a signal of greater power. This type of interference is known as multiple-access interference.

C. System Throughput Analysis

In a scenario with delay-limited transmission, the base station transmits messages to users at the predetermined data, and wireless fading channels affect system throughput. The TWR-associated NOMA's throughput can thus be expressed as

$$\mathcal{T}_{system} = \sum_{i=1}^{2} (1 - \mathcal{P}_{\mathrm{ID}i}) R_i. \quad (28)$$

D. Ergodic Data Analysis

In the latter scenario, when the IAP harvests energy from the PB's signal and uses it to carry the source signal to the destination, the ergodic data (ED) at the two IoT users are respectively calculated from

$$\mathcal{C}_{\mathrm{ID1}} \triangleq \mathbb{E}\left\{\log_2\left(1 + \min\left(\gamma_{\mathrm{IAP}}^{x_{\mathrm{ID1}}}, \gamma_{\mathrm{ID1}}^{x_{\mathrm{ID1}}}\right)\right)\right\}, \quad (29a)$$

$$\mathcal{C}_{\mathrm{ID2}} \triangleq \mathbb{E}\left\{\log_2\left(1 + \min\left(\gamma_{\mathrm{IAP}}^{x_{\mathrm{ID2}}}, \gamma_{\mathrm{ID2}}^{x_{\mathrm{ID2}}}\right)\right)\right\}, \quad (29b)$$

ED can be computed with numerical integration in (24) and deduced from the differential CDF in (26).

1) Ergodic Data of ID1: According to the definition of the expectation operator and after integration-by-part, $\mathcal{C}_{\mathrm{ID1}}$ can then be written as

$$C_{\mathrm{ID1}} = \frac{1}{\ln 2}\int_0^{\infty} \frac{1}{1+x} \bar{F}_{\hat{Z}_1}(x)dx, \quad (30)$$

where $\hat{Z}_1 = \min(\gamma_{\mathrm{IAP}}^{x_{\mathrm{ID1}}}, \gamma_{\mathrm{ID2}}^{x_{\mathrm{ID1}}})$ and $\bar{F}_{\hat{Z}_1}(x)$ denotes the complementary CDF, $\bar{F}_{\hat{Z}_1}(x) = 1 - F_{\hat{Z}_1}(x)$. The ergodic data of ID1

$$\mathcal{P}_{\mathrm{ID1}} = 1 - \psi \sum_{s=0}^{m_{h_1}-1}\sum_{a=0}^{s}\sum_{b=0}^{a}\binom{s}{a}\binom{a}{b} \frac{\zeta_1^s e^{-\frac{\zeta_1}{\lambda_{h_1}}} a_2^{a-b}\rho_S^{a-b}\rho_I^b \Gamma(m_{h_2}+a-b)\Gamma(Lm_{\mathrm{IAP}}+b)}{s!\lambda_{h_1}^s \delta_1^{m_{h_2}+a-b}\delta_2^{Lm_{\mathrm{IAP}}+b}}$$
$$\times \frac{1}{\Gamma(Lm_{\mathrm{ID1}})}\sum_{c=0}^{m_{h_0}-1}\sum_{r=0}^{Lm_{\mathrm{ID1}}-1}\binom{Lm_{\mathrm{ID1}}-1}{r}\frac{\phi_1 e^{\frac{1}{\lambda_{\mathrm{ID1}}\rho_I}}}{c!\Gamma(m_{g_1})(\lambda_{\mathrm{ID1}}\rho_I)^{Lm_{\mathrm{ID1}}-r-0.5m_{g_1}-0.5c-1}}$$
$$\times H_{1,0:0,2:1,1}^{0,1:2,0:0,1}\left(\left(1-\frac{2r+m_{g_1}+c+2}{2},1,1\right)\middle| \begin{matrix} - \\ \left(\frac{m_{g_1}-c}{2},1\right),\left(\frac{c-m_{g_1}}{2},1\right)\end{matrix}\middle|\begin{matrix}(1,1)\\(0,1)\end{matrix}\middle|\Theta^2\lambda_{\mathrm{ID1}}\rho_I, \rho_I\lambda_{\mathrm{ID1}}\right). \quad (24)$$

$$\mathcal{P}_{\mathrm{ID2}} = 1 - \psi \sum_{s=0}^{m_{h_1}-1}\sum_{a=0}^{s}\sum_{b=0}^{a}\sum_{c=0}^{m_{h_2}+a-b-1}\sum_{d=0}^{c}\binom{s}{a}\binom{a}{b}\binom{c}{d} \frac{\zeta_1^s e^{-\frac{\zeta_1}{\lambda_{h_1}}} a_2^{a-b}(m_{h_2}+a-b-1)!(Lm_{\mathrm{IAP}}+b+d-1)!}{s!c!\lambda_{h_1}^s \delta_1^{m_{h_2}+a-b-c}(\delta_2+\delta_1\zeta_2\rho_I)^{Lm_{\mathrm{IAP}}+b+d}}$$
$$\times \frac{\rho_S^{a-b}\rho_I^{b+d}\zeta_2^c e^{-\delta_1\zeta_2}}{\Gamma(Lm_{\mathrm{ID2}})}\sum_{c=0}^{m_{h_0}-1}\sum_{r=0}^{Lm_{\mathrm{ID2}}-1}\binom{Lm_{\mathrm{ID2}}-1}{r}\frac{\phi_2 e^{\frac{1}{\lambda_{\mathrm{ID2}}\rho_I}}}{c!\Gamma(m_{g_2})(\lambda_{\mathrm{ID2}}\rho_I)^{Lm_{\mathrm{ID2}}-r-0.5m_{g_2}-0.5c-1}}$$
$$\times H_{1,0:0,2:1,1}^{0,1:2,0:0,1}\left(\left(1-\frac{2r+m_{g_2}+c+2}{2},1,1\right)\middle| \begin{matrix} - \\ \left(\frac{m_{g_2}-c}{2},1\right),\left(\frac{c-m_{g_2}}{2},1\right)\end{matrix}\middle|\begin{matrix}(1,1)\\(0,1)\end{matrix}\middle|\Xi^2\lambda_{\mathrm{ID2}}\rho_I, \rho_I\lambda_{\mathrm{ID2}}\right), \quad (26)$$

for TWR-NOMA can be obtained from Proposition 3, described below.

Proposition 3: A closed-form approximate expression of ED for ID1 is given by (31), shown at the bottom of this page, in which $\tilde{\Theta}(t) = \sqrt{\frac{t}{\lambda_{h_0}\lambda_{g_1}b_1\theta}}$, $\tilde{\delta}_1(t) = (\frac{1}{\lambda_{h_2}} + \frac{a_2\rho_S t}{a_1\rho_S\lambda_{h_1}})$, $\tilde{\delta}_2(t) = (\frac{1}{\lambda_{\text{IAP}}} + \frac{\rho_I t}{a_1\rho_S\lambda_{h_1}})$, $\mathcal{G}(t) = \tan(\frac{\pi(t+1)}{4})$ and $\upsilon_m = \cos(\frac{2m-1}{2M}\pi)$.

Proof: See Appendix C, available online.

2) Ergodic Data of ID2: Similarly, $\mathcal{C}_{\text{ID2}}$ can then be written as

$$\mathcal{C}_{\text{ID2}} = \frac{1}{\ln 2}\int_0^{b_2/b_1} \frac{1}{1+x}\bar{F}_{\hat{Z}_2}\left(\frac{x}{b_2 - xb_1}\right)dx, \tag{32}$$

where $\hat{Z}_2 = \min(\gamma_{\text{IAP}}^{x_{\text{ID2}}}, \gamma_{\text{ID2}}^{x_{\text{ID2}}})$ and $\bar{F}_{\hat{Z}_2}(x)$ denotes the complementary CDF, $\bar{F}_{\hat{Z}_2}(x) = 1 - F_{\hat{Z}_2}(x)$.

Proposition 4: A closed-form approximated expression of ED for ID2 is given by (33), shown at the bottom of this page, in which $\xi_2(t) = \frac{t}{\theta(b_2 - tb_1)}$, $\Xi(t) = \sqrt{\frac{\xi_2(t)}{\lambda_{h_0}\lambda_{g_2}}}$, $\phi_2(t) = (-1)^{Lm_{\text{ID2}}-r-1}\Xi(t)^{m_{g_2}+c}$ $\Psi(t) = \frac{a_2(t+1)}{2a_1}$ and $\upsilon_q = \cos(\frac{2q-1}{2Q}\pi)$.

Proof: See Appendix D, available online.

E. Optimal Power Allocation and EH Time Coefficients

This section presents an iterative search algorithm for determining the optimal values of the power allocation coefficient (a_2) and EH time coefficient (α) for minimizing the outage probability. Specifically, the 2D Golden Section Search (GSS) algorithm [62] is employed to solve this problem. This algorithm can repeatedly update its search to obtain the optimal values of a_2^* and α^* (see Algorithm 1). The 2D GSS algorithm applies an effective strategy by updating intermediate locations based on the golden ratio and uses fewer iterations than other algorithms [63]. When the intermediate points are modified, the 2D GSS algorithm simply requires a new calculation. The 2D GSS is thus an ideal algorithm for determining optimal points before data transfer is executed.

IV. Performance Prediction Based on a DNN

In this section, we design and suggest a DNN to predict the outage probability of two IoT users simultaneously with quick execution and low computational complexity toward real-time estimation, whereas the conventional analysis and Monte Carlo simulations are constrained or take a long time if IoT users are changed. Additionally, an analysis and evaluation of the effects of such characteristics on network architecture and system performance is conducted.

A. Structure of the DNN

This section describes the DNN structure, which includes an input layer, hidden layer, and output layer, for a TWR-NOMA network (Fig. 3). The input layer contains 18 neurons; Table II lists the parameters. Each hidden layer $k(k = 1,\ldots, D_{\text{hiden}})$ includes a rectified linear unit (ReLU) activation function to perform a threshold operation on each input element, where D_{hiden} denotes the number of hidden layers and contains D_{neuron}^k neurons. The single neuron output layer produces the expected outage performance. The estimated outage probability $\mathcal{P}_{\text{IDi}}$ is calculated from the linear and activation functions [64], [65].

The training and prediction phases are two parts of the training process in the proposed method. The adaptive moment

$$\begin{aligned}\mathcal{C}_{\text{ID1}} \approx {} & \frac{\pi^2\psi}{4M\ln 2}\sum_{s=0}^{m_{h_1}-1}\sum_{a=0}^{s}\sum_{b=0}^{a}\binom{s}{a}\binom{a}{b}\frac{a_2^{a-b}\rho_S^{a-b}\rho_I^b\Gamma(m_{h_2}+a-b)\Gamma(Lm_{\text{IAP}}+b)}{s!\lambda_{h_1}^s\Gamma(Lm_{\text{ID1}})}\sum_{c=0}^{m_{h_0}-1}\sum_{r=0}^{Lm_{\text{ID1}}-1}\sum_{m=1}^{M}\binom{Lm_{\text{ID1}}-1}{r}\\
&\times\frac{(-1)^{Lm_{\text{ID1}}-r-1}e^{\frac{1}{\lambda_{\text{ID1}}\rho_I}}\sqrt{1-\upsilon_m^2}\sec^2\left(\frac{\pi(\upsilon_m+1)}{4}\right)\mathcal{G}(\upsilon_m)^s e^{-\frac{\mathcal{G}(\upsilon_m)}{a_1\lambda_{h_1}\rho_S}}\tilde{\Theta}[\mathcal{G}(\upsilon_m)]^{m_{g_1}+c}}{c!\Gamma(m_{g_1})(\lambda_{\text{ID1}}\rho_I)^{Lm_{\text{ID1}}-r-0.5m_{g_1}-0.5c-1}a_1^s\rho_S^s[1+\mathcal{G}(\upsilon_m)]\tilde{\delta}_1[\mathcal{G}(\upsilon_m)]^{m_{h_2}+a-b}\tilde{\delta}_2[\mathcal{G}(\upsilon_m)]^{Lm_{\text{IAP}}+b}}\\
&\times H_{1,0:0,2:1,1}^{0,1:2,0:0,1}\left(\begin{matrix}\left(1-\frac{2r+m_{g_1}+c+2}{2},1,1\right)\\ -\end{matrix}\middle|\begin{matrix}-\\ \left(\frac{m_{g_1}-c}{2},1\right),\left(\frac{c-m_{g_1}}{2},1\right)\end{matrix}\middle|\begin{matrix}(1,1)\\(0,1)\end{matrix}\middle|\tilde{\Theta}[\mathcal{G}(\upsilon_m)]^2\lambda_{\text{ID1}}\rho_I,\rho_I\lambda_{\text{ID1}}\right).\end{aligned}\tag{31}$$

$$\begin{aligned}\mathcal{C}_{\text{ID2}} \approx {} & \frac{\pi a_2}{2Qa_1\ln 2\Gamma(Lm_{\text{IAP}})\lambda_{\text{IAP}}^{Lm_{\text{IAP}}}}\sum_{s=0}^{m_{h_2}-1}\sum_{a=0}^{s}\binom{s}{a}\frac{\rho_I^a\Gamma(Lm_{\text{IAP}}+a)}{s!\lambda_{h_2}^s a_2^s\rho_S^s\Gamma(Lm_{\text{ID2}})}\sum_{c=0}^{m_{h_0}-1}\sum_{r=0}^{Lm_{\text{ID2}}-1}\binom{Lm_{\text{ID2}}-1}{r}\\
&\times\frac{\Psi(\upsilon_q)^s\phi_2[\Psi(\upsilon_q)]e^{\frac{1}{\lambda_{\text{ID2}}\rho_I}}}{c!\Gamma(m_{g_2})(\lambda_{\text{ID2}}\rho_I)^{Lm_{\text{ID2}}-r-0.5m_{g_2}-0.5c-1}[1+\Psi(\upsilon_q)]\hat{\delta}_2[\Psi(\upsilon_q)]^{Lm_{\text{IAP}}+a}}e^{-\frac{\Psi(\upsilon_q)}{\lambda_{h_2}a_2\rho_S}}\sum_{q=1}^{Q}\sqrt{1-\upsilon_q^2}\\
&\times H_{1,0:0,2:1,1}^{0,1:2,0:0,1}\left(\begin{matrix}\left(1-\frac{2r+m_{g_2}+c+2}{2},1,1\right)\\ -\end{matrix}\middle|\begin{matrix}-\\ \left(\frac{m_{g_2}-c}{2},1\right),\left(\frac{c-m_{g_2}}{2},1\right)\end{matrix}\middle|\begin{matrix}(1,1)\\(0,1)\end{matrix}\middle|\Xi[\Psi(\upsilon_q)]^2\lambda_{\text{ID2}}\rho_I,\rho_I\lambda_{\text{ID2}}\right).\end{aligned}\tag{33}$$

Algorithm 1: Optimization Algorithm to Find a_2^* and α^* Based on a 2D Golden Section Search.

Input: Establish $[\psi_{\min}, \psi_{\max}] = [\vartheta_{\min}, \vartheta_{\max}] = [0, 1]$, the interval parameters $\varpi_{a_2} = \frac{\sqrt{5}-1}{2}(\psi_{\max} - \psi_{\min})$, $\varpi_{\alpha} = \frac{\sqrt{5}-1}{2}(\vartheta_{\max} - \vartheta_{\min})$ and the stopping threshold $\Lambda_{a_2} = \Lambda_{\alpha} = 10^{-4}$

Output: The optimal of a_2^* and α^* that minimum the outage performance $\mathcal{P}_{\text{IDi}}(a_2^*, \alpha)$, $i \in \{1, 2\}$

1: *Initialization:* $\psi_1 = \psi_{\min} + \varpi_{a_2}$, $\psi_2 = \psi_{\max} - \varpi_{a_2}$, $\vartheta_1 = \vartheta_{\min} + \varpi_{\alpha}$ and $\vartheta_2 = \vartheta_{\max} - \varpi_{\alpha}$
2: **while** $|\psi_{\max} - \psi_{\min}| \leq \Lambda_{a_2}$ NOR $|\vartheta_{\max} - \vartheta_{\min}| \leq \Lambda_{\alpha}$ **do**
3: **if** $\mathcal{P}_{\text{IDi}}(\psi_1, \vartheta_1)$ is the minimum in the following cases: $\mathcal{P}_{\text{IDi}}(\psi_1, \vartheta_1)\mathcal{P}_{\text{IDi}}(\psi_1, \vartheta_2)\mathcal{P}_{\text{IDi}}(\psi_2, \vartheta_1)\mathcal{P}_{\text{IDi}}(\psi_2, \vartheta_2)$ **then**
4: Update: $\psi_{\min} = \psi_2$, $\psi_2 = \psi_1$, $\psi_{\max} = \psi_{\max}$, $\psi_1 = \psi_{\min} + \varpi_{a_2}$, $\vartheta_{\min} = \vartheta_2$, $\vartheta_2 = \vartheta_1$, $\vartheta_{\max} = \vartheta_{\max}$, $\vartheta_1 = \vartheta_{\min} + \varpi_{\alpha}$
5: **else if** $\mathcal{P}_{\text{IDi}}(\psi_1, \vartheta_2)$ is the minimum in the following cases: $\mathcal{P}_{\text{IDi}}(\psi_1, \vartheta_1)\mathcal{P}_{\text{IDi}}(\psi_1, \vartheta_2)\mathcal{P}_{\text{IDi}}(\psi_2, \vartheta_1)\mathcal{P}_{\text{IDi}}(\psi_2, \vartheta_2)$ **then**
6: Update: $\psi_{\min} = \psi_2$, $\psi_2 = \psi_1$, $\psi_{\max} = \psi_{\max}$, $\psi_1 = \psi_{\min} + \varpi_{a_2}$, $\vartheta_{\min} = \vartheta_{\min}$, $\vartheta_{\max} = \vartheta_1$, $\vartheta_1 = \vartheta_2$, $\vartheta_2 = \vartheta_{\max} - \varpi_{\alpha}$
7: **else if** $\mathcal{P}_{\text{IDi}}(\psi_2, \vartheta_1)$ is the minimum in the following cases: $\mathcal{P}_{\text{IDi}}(\psi_1, \vartheta_1)$, $\mathcal{P}_{\text{IDi}}(\psi_1, \vartheta_2)$, $\mathcal{P}_{\text{IDi}}(\psi_2, \vartheta_1)$, $\mathcal{P}_{\text{IDi}}(\psi_2, \vartheta_2)$ **then**
8: Update: $\psi_{\min} = \psi_{\min}$, $\psi_{\max} = \psi_1$, $\psi_1 = \psi_2$, $\psi_2 = \psi_{\max} - \varpi_{a_2}$, $\vartheta_{\min} = \vartheta_2$, $\vartheta_2 = \vartheta_1$, $\vartheta_{\max} = \vartheta_{\max}$, $\vartheta_1 = \vartheta_{\min} + \varpi_{\alpha}$
9: **else**
10: Update: $\psi_{\min} = \psi_{\min}$, $\psi_{\max} = \psi_1$, $\psi_1 = \psi_2$, $\psi_2 = \psi_{\max} - \varpi_{a_2}$, $\vartheta_{\min} = \vartheta_{\min}$, $\vartheta_{\max} = \vartheta_1$, $\vartheta_1 = \vartheta_2$, $\vartheta_2 = \vartheta_{\max} - \varpi_{\alpha}$
11: **end if**
12: **end while**
13: **return** The minimum of the outage probability $\mathcal{P}_{\text{IDi}}(\frac{\psi_{\min}+\psi_{\max}}{2}, \frac{\vartheta_{\min}+\vartheta_{\max}}{2})$

estimation (Adam) optimization approach, which attempts to maximize the model parameters depending on the dataset, can be used to teach the network input-output relations offline during the training phase. This process computes biases and updates weights iteratively throughout the backpropagation procedure and is complete after calculating the loss function. To predict OP during the communications process, it is important to point out that this part is performed only once, but it can also be applied multiple times. In the next part, the outputs from the offline training model are used to forecast the OP online whenever fresh data is available at the input. Because the training step is completed offline, the computational complexity, implementation cost, and execution time can be greatly reduced.

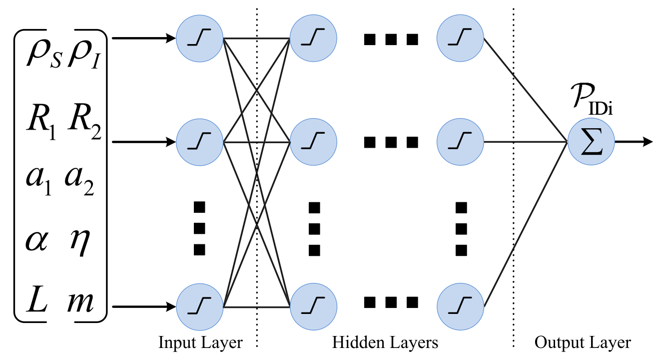

Fig. 3. Proposed DNN model for OP prediction.

TABLE II
INPUTS FOR DNN TESTING AND TRAINING

Inputs	Values	Inputs	Values
ρ_S	[0:5:50]	α	0.2
a_1	0.9	ρ_I	10 dB
a_2	0.1	λ_{h_0}	1
η	0.8	λ_{h_1}	1
L	[2,4]	λ_{h_2}	1
R_1	1.1	λ_{g_1}	1
R_2	1.1	λ_{g_2}	1
m	[1,2]	λ_{ID1}	0.5
λ_{IAP}	0.5	λ_{ID2}	0.5

B. Dataset

The TWR-NOMA system's parameters are generated uniformly based on the network's size and extracted as input variables of the training samples. In a real scenario, the TWR-NOMA system is able to accumulate the dataset over a long period. However, the simulation in the current study employed sufficient samples to produce highly precise estimates for outage performance. The generated dataset $\mathcal{J}$ contains k samples, each of which is a row vector where $\text{Data}[k] = [\mathbf{t}[k], \mathcal{P}_{\text{out}}^{\text{Sim}}]$, and $\mathbf{t}[i]$ is feature vector which contains all the input parameters specified in Table II. The dataset is employed to build real-value OP sets from a Monte Carlo simulation and return a unique $\mathcal{P}_{\text{out}}^{\text{Sim}}$. For the purposes of the study, 10^5 data samples were generated, combined, and then divided into a new dataset comprising 80% for $\mathcal{J}_{\text{trn}}$, 10% for $\mathcal{J}_{\text{vali}}$ and 10% for $\mathcal{J}_{\text{test}}$, where $\mathcal{J}_{\text{trn}}$, $\mathcal{J}_{\text{vali}}$ and $\mathcal{J}_{\text{test}}$ Note that data training, data validation and data testing, respectively.

The suggested DNN model's estimation accuracy was calculated from the mean-square error (MSE), which is formally expressed as

$$\text{MSE} = \frac{1}{|\mathcal{J}_{\text{tes}}|} \sum_{i=0}^{|\mathcal{J}_{\text{tes}}|-1} \left(\mathcal{P}_{\text{out}}[1] - \mathcal{P}_{\text{out}}^{\text{tes}}\right)^2. \tag{34}$$

The root-mean-square error (RMSE) calculates the differences between the real OP values and predicted OP values over the entire test set for the purpose of assessing the estimation performance of the proposed DNN model in predicting the OP. Note that RMSE can be expressed as $\text{RMSE} = \sqrt{\text{MSE}}$.

TABLE III
SYSTEM PARAMETERS FOR EVALUATING SCENARIOS

Parameters	Values
a_1, a_2	$\{0.9, 0.1\}$
α, η	$\{0.2, 0.8\}$
R_1, R_2	$\{1.1, 1.1\}$
m	5
ρ_I	5 dB
L	4
$\lambda_{h_0}, \lambda_{h_1}, \lambda_{h_2}, \lambda_{g_1}, \lambda_{g_2}$	$\{1, 1, 1, 1, 1\}$
$\lambda_{\text{IAP}}, \lambda_{\text{ID1}}, \lambda_{\text{ID2}}$	$\{0.5, 0.5, 0.5\}$

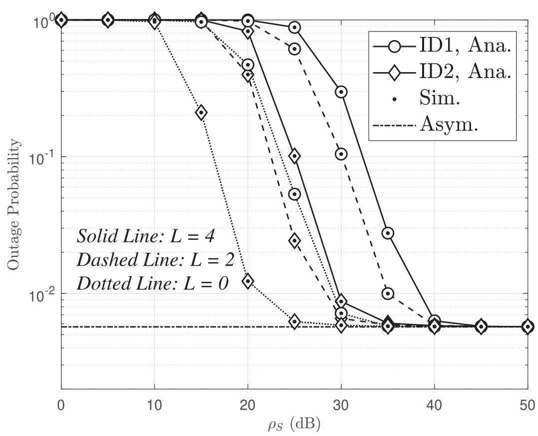

Fig. 4. Outage probability of EH TW-NOMA in the presence of co-channel interference.

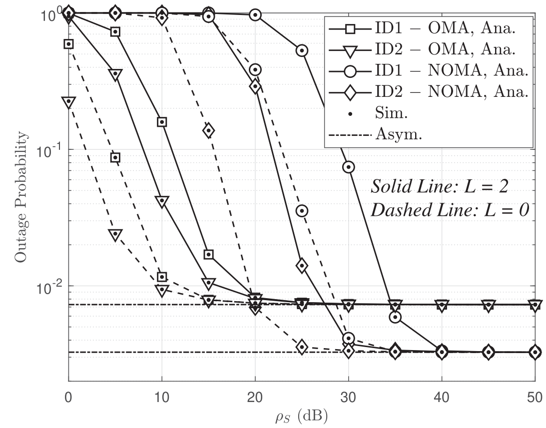

Fig. 5. Comparison between NOMA and OMA: Outage probability versus ρ_S(dB).

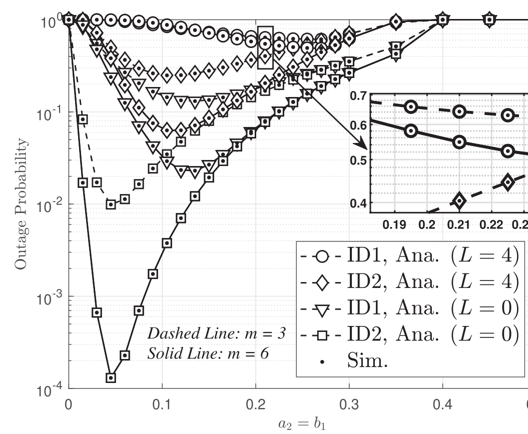

Fig. 6. Outage probability versus power allocation factor a_2 and b_1, with $\rho = 25$ dB.

V. NUMERICAL RESULTS

This section quantitatively assesses the theoretical results for OP performance. The fading parameters were set to $m = m_{h_0} = m_{h_1} = m_{h_2} = m_{g_1} = m_{g_2} = m_{\text{IAP}} = m_{\text{ID1}} = m_{\text{ID2}}$. The results of the Monte Carlo simulation were averaged across 10^6 separate trials. The term BPCU for the goal rate refers to bit per channel user. Monte-Carlo simulation and asymptotic computation-based simulation, respectively. Furthermore, The DNN model consists 5 hidden layers comprised of 100 neurons per layer with 70 epochs of training. The experiments are carried out on a Laptop with an Intel Core i5, Nvidia GeForce RTX-4050, and Python 3.7.9 related to Keras 2.3.1. Table III provides a summary of other vital parameters. In addition, the Gauss-Chebyshev parameter was set to $M = Q = 100$ to yield an accurate approximation [66].

Fig. 4 plots the outage probability of two users ID1 and ID2 versus ρ_S (dB) at different levels of interference. Fig. 4 shows that the results of the Monte Carlo simulation clearly match the outage probability curves. The asymptotic outage probability for two users is also plotted according to (27). In the high SNR regime, the asymptotic outage probability closely matches the simulated outage probabilities. Error floors are always present for the two users, and accordingly, the diversity orders are all zero. Because inter-user interference is inherent in NOMA, the outage probability still has an error floor. Increasing the level of interference also significantly degrades the outage probability performance of the two users in the low ρ_S regime. As can be observed in Fig. 5, the outage performance of two users in the NOMA scheme is superior to the OMA scheme in the low SNR regime in two cases $L = 0$ and $L = 2$. This is due to the two users exchanging the information in four-time slots in the OMA scheme. Therefore, it requires a larger SNR value to achieve the same target as the NOMA scheme. In addition, the outage probability of two users in the NOMA scheme is limited by inter-user interference. The OMA scheme is just limited by the noise signal. Thus, the OMA scheme outperforms the NOMA scheme in the high SNR region.

Fig. 6 confirms the power allocation system influencing the OPs of two users. It is worth noting that user ID2's OP is mostly dependent on $a_2 = b_1$. When $a_2 = b_1$ is from 0 to 0.3, user ID2's outage performance improves substantially more than user ID1, but it then deteriorates. The fundamental reason for this is that $a_2 = b_1$ plays a significant part in affecting SINR values, which causes the corresponding OPs to change. Furthermore, when increasing L means increasing the number of interferences, we must increase the power allocation coefficient to get a better OP value according to the OP formula (24) and (26). Fig. 7 shows the outage probability versus ρ_S(dB) with a varying channel m parameter and compares the outage probabilities of two

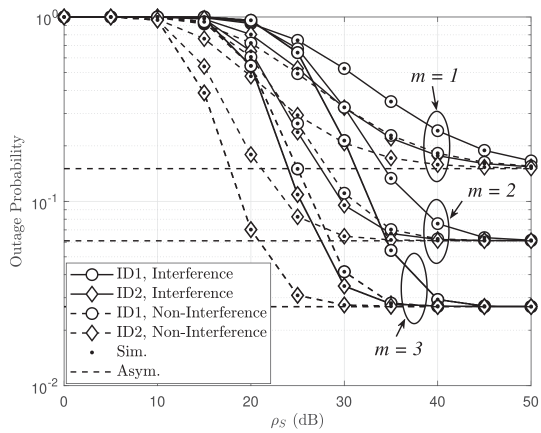

Fig. 7. Outage probability of EH TWR-NOMA in the presence of co-channel interference.

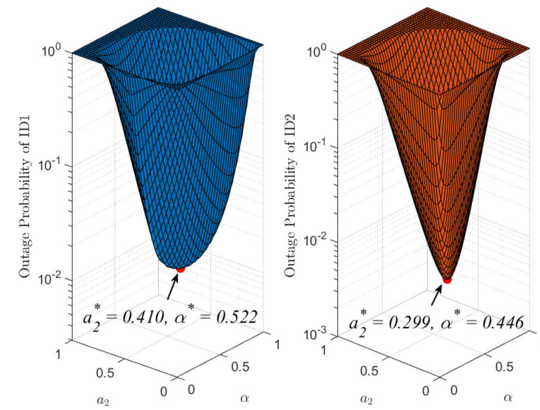

Fig. 9. Outage probability of two users versus α and a_2 when $L = 2, m = 5$, $R_1 = R_2 = 0.1$, $\rho_I = 10$ dB, and $\rho_S = 15$ dB.

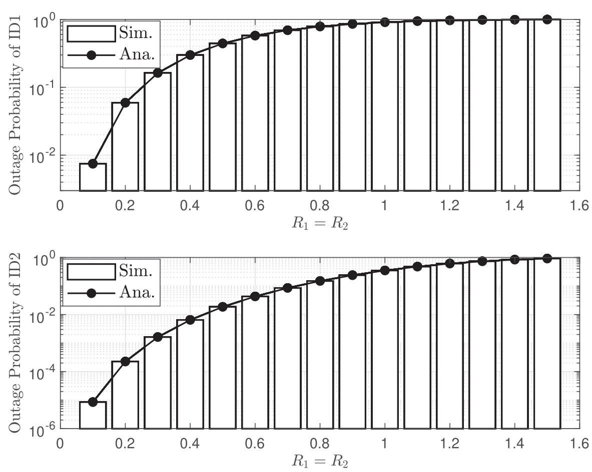

Fig. 8. Outage probability of two users versus R_1 and R_2 under $L = 2$, $m = 5$, $\alpha = 0.3$, $a_1 = 0.9$, $a_2 = 0.1$, and $\rho_S = 20$ dB.

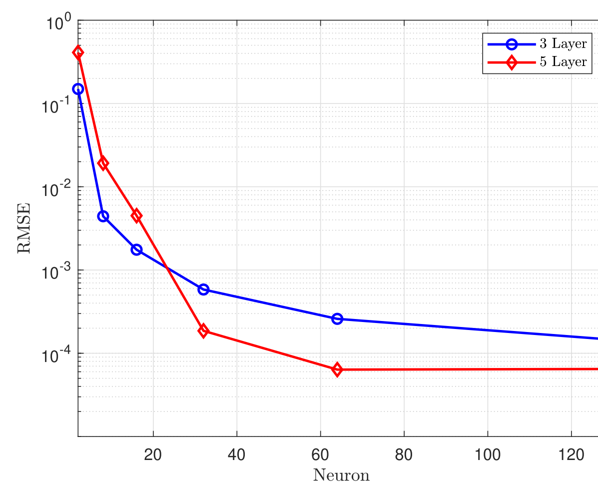

Fig. 10. MSE convergence in validating and training the DNN.

users with interference ($L = 2$) and non-interference ($L = 0$). At $m = 1$, Rayleigh fading can be applied on all channels. Outage probability clearly improved as parameter m increased. The outage probability of the two users improved significantly in non-interference cases. Fig. 8 shows the outage probability of two users IDi versus $R_1 = R_2$ and indicates that the outage probability of the two users increased as the target rate of two users $R_1 = R_2$ increased; target rates are conditions which limit the outage probability performance.

Fig. 9 analyzes the relationship between the value α and the power allocation coefficient a_2 and the outage probabilities of the two users. The outage probabilities for the transmission SNR and power allocation coefficients clearly represent a convex function. The 2D GSS technique described in Section III can therefore be applied to select the best values of α and a_2 to reduce the outage probability. Applying the 2D GSS method, the optimal values of α and a_2 were 0.552 and 0.410 for the outage probability of ID1. For the outage probability of ID2, the best values of α and a_2 were 0.446 and 0.299, respectively. In addition, the optimal values of the power allocation coefficient a_1^* were $a_1^* = 1 - a_2^*$.

Fig. 10 charts the RMSE of the proposed DNN model versus neurons with a varying number of hidden layers. The generated DNN model was applied to predict the OP of the TWR-NOMA system. The graph clearly indicates that as the number of hidden layers increased, the estimated RMSE of the OP was smaller. This was a result of the DNN model having numerous hidden layers capable of generalizing the dataset, thereby producing an increase in network capacity. Fig. 11 demonstrates how the DNN is able to forecast the outage probability of two users and indicates the similarity of the projected values of the outage behavior to the outage probability obtained from Monte Carlo simulations. Because the outage performance of the two users is determined by the IAP's allocation of transmitted power to the users' signals, the IAP is able to forecast outage behavior and alter the power allocation parameters to satisfy user fairness or other conditions.

Fig. 12 displays the system throughput for two schemes in relation to the various values of α and η. It is interesting to note that, as the initial discovery in (2) shows, the throughput

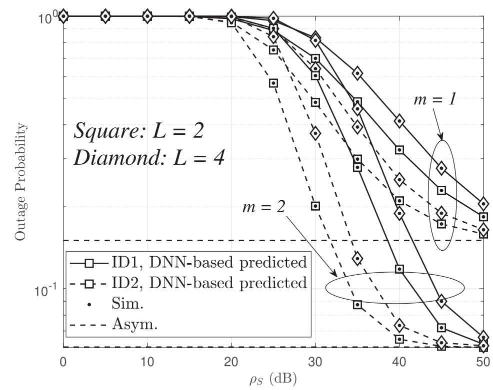

Fig. 11. Comparison between the predicted outage performance and analytical simulations under different L.

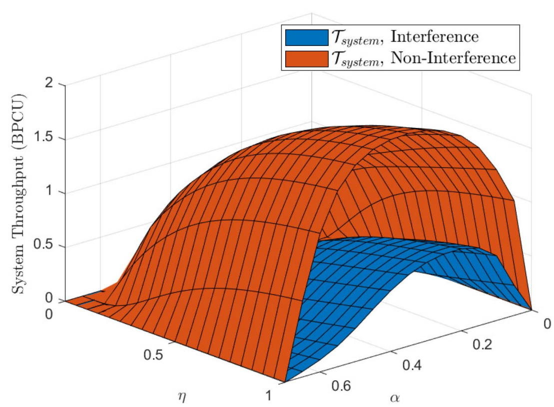

Fig. 12. System throughput versus α and η when $L = 2$, $m = 4$, $a_1 = 0.9$, $a_2 = 0.1$, $R_1 = R_2 = 1.1$, $\rho_S = 10$ dB, and $\rho_I = 5$ dB.

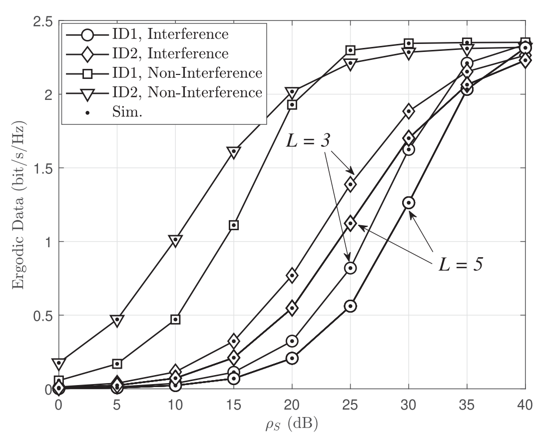

Fig. 13. ED versus transmission ρ_S, with $m = 4$, $a_1 = 0.8$, $a_2 = 0.2$, and $\rho_I = 10$ dB.

system changes dramatically and depends on energy harvesting procedure settings at the IAP. In the non-interference case, system throughput also improved significantly. However, because of the effect of CCI on the SINR of the proposed system, throughput deteriorated significantly. When energy conversion efficiency was greater, system throughput also increased. When α increased to approximately 0.4 regions, system throughput increased, but when alpha was larger, throughput decreased. Also, changing the power of the IPA with coefficient α led to a change in the SINR and consequently a change in the system's outage probability and throughput. Fig. 13 graphs the ED as a function of transmission ρ_S(dB). Generally, it can be seen that a rise in ρ_S(dB) enhances the ED at the user. The ED at the two users are nearly equal at lower SNR values of approximately -10 dB. Once the SNR rises beyond 40 dB, the ergodic data curves become saturated because of the effect of interference on the SINR.

VI. Conclusion

This study has investigated a novel TWR-NOMA-enabled IoT network with CCI and an IAP assisted by a PB using a TS protocol developed to improve spectral efficiency. Monte Carlo simulations were used to derive and validate the developed closed-form analytical equations for the OP and ED for two users and system throughput. Using these equations, diversity orders of zero were obtained with inter-user interference among stacked NOMA signals. To improve the outage performance of the two users, the proposed algorithm applied low complexity 2D GSS to reduce the user's OP via a jointly optimal TS and two power allocation factors. The numerical results showed that as the CCI increased, outage performance at the user dramatically decreased. A deep learning strategy was created as a novel method for forecasting outage probability with high accuracy and low computing complexity. Using DNN prediction, the outage probability results closely approximated the Monte-Carlo simulation and the results of numerical analysis. A DNN is therefore a potentially promising and efficient technique for evaluating system performances through a low-latency inference process which avoids the derivation of complicated closed-form expressions for practical network scenarios.

References

[1] D.-H. Tran, V.-D. Nguyen, S. Chatzinotas, T. X. Vu, and B. Ottersten, "UAV relay-assisted emergency communications in IoT networks: Resource allocation and trajectory optimization," *IEEE Trans. Wireless Commun.*, vol. 21, no. 3, pp. 1621–1637, Mar. 2022.

[2] M. R. Palattella et al., "Internet of Things in the 5G era: Enablers, architecture, and business models," *IEEE J. Sel. Areas Commun.*, vol. 34, no. 3, pp. 510–527, Mar. 2016.

[3] Z. Sheng, S. Yang, Y. Yu, A. V. Vasilakos, J. A. Mccann, and K. K. Leung, "A survey on the IETF protocol suite for the Internet-of-Things: Standards, challenges and opportunities," *IEEE Wireless Commun.*, vol. 20, no. 6, pp. 91–98, Dec. 2013.

[4] P. X. Nguyen et al., "Backscatter-assisted data offloading in OFDMA-Based wireless-powered mobile edge computing for IoT networks," *IEEE Internet Things J.*, vol. 8, no. 11, pp. 9233–9243, Jun. 2021.

[5] M. Shirvanimoghaddam, M. Dohler, and S. J. Johnson, "Massive non-orthogonal multiple access for cellular IoT: Potentials and limitations," *IEEE Commun. Mag.*, vol. 55, no. 9, pp. 55–61, Sep. 2017.

[6] T. D. Hieu et al., "Stability-aware geographic routing in energy harvesting wireless sensor networks," *Sensors*, vol. 16, no. 5, 2016, Art. no. 696.

[7] A. Ö. Ercan, M. O. Sunay, and I. F. Akyildiz, "RF energy harvesting and transfer for spectrum sharing cellular IoT communications in 5G systems," *IEEE Trans. Mobile Comput.*, vol. 17, no. 7, pp. 1680–1694, Jul. 2018.

[8] J. Hu, K. Yang, G. Wen, and L. Hanzo, "Integrated data and energy communication network: A comprehensive survey," *IEEE Commun. Surv. Tut.*, vol. 20, no. 4, pp. 3169–3219, Fourth Quarter 2018.

[9] T. N. Nguyen et al., "Security–reliability tradeoff analysis for SWIPT- and AF-based IoT networks with friendly jammers," *IEEE Internet Things J.*, vol. 9, no. 21, pp. 21662–21675, Nov. 2022.

[10] D. Ma, G. Lan, M. Hassan, W. Hu, and S. K. Das, "Sensing, computing, and communications for energy harvesting IoTs: A survey," *IEEE Commun. Surv. Tut.*, vol. 22, no. 2, pp. 1222–1250, Second Quarter 2020.

[11] K. W. Choi, P. A. Rosyady, L. Ginting, A. A. Aziz, D. Setiawan, and D. I. Kim, "Theory and experiment for wireless-powered sensor networks: How to keep sensors alive," *IEEE Trans. Wireless Commun.*, vol. 17, no. 1, pp. 430–444, Jan. 2018.

[12] X. Lu, P. Wang, D. Niyato, D. I. Kim, and Z. Han, "Wireless networks with RF energy harvesting: A contemporary survey," *IEEE Commun. Surv. Tut.*, vol. 17, no. 2, pp. 757–789, Second Quarter 2015.

[13] D.-H. Tran, S. Chatzinotas, and B. Ottersten, "Throughput maximization for backscatter- and cache-assisted wireless powered UAV technology," *IEEE Trans. Veh. Technol.*, vol. 71, no. 5, pp. 5187–5202, May 2022.

[14] I. Krikidis, S. Timotheou, S. Nikolaou, G. Zheng, D. W. K. Ng, and R. Schober, "Simultaneous wireless information and power transfer in modern communication systems," *IEEE Commun. Mag.*, vol. 52, no. 11, pp. 104–110, Nov. 2014.

[15] B. Clerckx, R. Zhang, R. Schober, D. W. K. Ng, D. I. Kim, and H. V. Poor, "Fundamentals of wireless information and power transfer: From RF energy harvester models to signal and system designs," *IEEE J. Sel. Areas Commun.*, vol. 37, no. 1, pp. 4–33, Jan. 2019.

[16] T. N. Nguyen, T. T. Duy, P. T. Tran, and M. Voznak, "Performance evaluation of user selection protocols in random networks with energy harvesting and hardware impairments," *Adv. Elect. Electron. Eng.*, vol. 14, no. 4, pp. 372–377, 2016.

[17] T. D. Ponnimbaduge Perera, D. N. K. Jayakody, S. K. Sharma, S. Chatzinotas, and J. Li, "Simultaneous wireless information and power transfer (SWIPT): Recent advances and future challenges," *IEEE Commun. Surv. Tut.*, vol. 20, no. 1, pp. 264–302, First Quarter 2018.

[18] D.-T. Do, C.-B. Le, and A.-T. Le, "Joint of full-duplex relay, non-linear energy harvesting and multiple access in performance improvement of cell-edge user in heterogeneous networks," *Wireless Netw.*, vol. 26, pp. 6253–6266, 2020.

[19] T. N. Nguyen et al., "Physical layer security in AF-Based cooperative SWIPT sensor networks," *IEEE Sensors J.*, vol. 23, no. 1, pp. 689–705, Jan. 2023.

[20] D.-T. Do, A.-T. Le, Y. Liu, and A. Jamalipour, "User grouping and energy harvesting in UAV-NOMA system with AF/DF relaying," *IEEE Trans. Veh. Technol.*, vol. 70, no. 11, pp. 11855–11868, Nov. 2021.

[21] T. M. Hoang et al., "Performance analysis of power beacon-assisted energy harvesting NOMA multi-user relaying system over Nakagami-m fading channels," *AEU- Int. J. Electron. Commun.*, vol. 115, 2020, Art. no. 153022.

[22] K. Huang and V. K. N. Lau, "Enabling wireless power transfer in cellular networks: Architecture, modeling and deployment," *IEEE Trans. Wireless Commun.*, vol. 13, no. 2, pp. 902–912, Feb. 2014.

[23] S. Nikoletseas, T. P. Raptis, and C. Raptopoulos, "Low radiation efficient wireless energy transfer in wireless distributed systems," in *Proc. IEEE 35th Int. Conf. Distrib. Comput. Syst.*, 2015, pp. 196–204.

[24] R. Dai et al., "Robustly safe charging for wireless power transfer," in *Proc. IEEE Conf. Comput. Commun.*, 2018, pp. 378–386.

[25] T. D. Hieu, T. T. Duy, and B.-S. Kim, "Performance enhancement for multihop harvest-to-transmit WSNs with path-selection methods in presence of eavesdroppers and hardware noises," *IEEE Sensors J.*, vol. 18, no. 12, pp. 5173–5186, Jun. 2018.

[26] M. Vaezi, R. Schober, Z. Ding, and H. V. Poor, "Non-orthogonal multiple access: Common myths and critical questions," *IEEE Wireless Commun.*, vol. 26, no. 5, pp. 174–180, Oct. 2019.

[27] Z. Ding, J. Xu, O. A. Dobre, and H. V. Poor, "Joint power and time allocation for NOMA–MEC offloading," *IEEE Trans. Veh. Technol.*, vol. 68, no. 6, pp. 6207–6211, Jun. 2019.

[28] D.-T. Do and A.-T. Le, "NOMA based cognitive relaying: Transceiver hardware impairments, relay selection policies and outage performance comparison," *Comput. Commun.*, vol. 146, pp. 144–154, 2019.

[29] Z. Ding, M. Peng, and H. V. Poor, "Cooperative non-orthogonal multiple access in 5G systems," *IEEE Commun. Lett.*, vol. 19, no. 8, pp. 1462–1465, Aug. 2015.

[30] Z. Ding, Z. Yang, P. Fan, and H. V. Poor, "On the performance of non-orthogonal multiple access in 5G systems with randomly deployed users," *IEEE Signal Process. Lett.*, vol. 21, no. 12, pp. 1501–1505, Dec. 2014.

[31] M. Vaezi, Z. Ding, and H. V. Poor, *Multiple Access Techniques for 5G Wireless Networks and Beyond*, vol. 159. Berlin, Germany: Springer, 2019.

[32] X. Li et al., "Hardware impaired ambient backscatter NOMA systems: Reliability and security," *IEEE Trans. Commun.*, vol. 69, no. 4, pp. 2723–2736, Apr. 2021.

[33] X. Li et al., "Physical-layer authentication for ambient backscatter-aided NOMA symbiotic systems," *IEEE Trans. Commun.*, vol. 71, no. 4, pp. 2288–2303, Apr. 2023.

[34] R. Zhang, Y.-C. Liang, C. C. Chai, and S. Cui, "Optimal beamforming for two-way multi-antenna relay channel with analogue network coding," *IEEE J. Sel. Areas Commun.*, vol. 27, no. 5, pp. 699–712, Jun. 2009.

[35] R. Vaze and R. W. Heath, "On the capacity and diversity-multiplexing tradeoff of the two-way relay channel," *IEEE Trans. Inf. Theory*, vol. 57, no. 7, pp. 4219–4234, Jul. 2011.

[36] Y.-U. Jang and Y. H. Lee, "Performance analysis of user selection for multiuser two-way amplify-and-forward relay," *IEEE Commun. Lett.*, vol. 14, no. 11, pp. 1086–1088, Nov. 2010.

[37] B. Zheng, X. Wang, M. Wen, and F. Chen, "NOMA-Based multi-pair two-way relay networks with rate splitting and group decoding," *IEEE J. Sel. Areas Commun.*, vol. 35, no. 10, pp. 2328–2341, Oct. 2017.

[38] L. Lv, Q. Ye, Z. Ding, Z. Li, N. Al-Dhahir, and J. Chen, "Multi-antenna two-way relay based cooperative NOMA," *IEEE Trans. Wireless Commun.*, vol. 19, no. 10, pp. 6486–6503, Oct. 2020.

[39] M. A. Al-Garadi, A. Mohamed, A. K. Al-Ali, X. Du, I. Ali, and M. Guizani, "A survey of machine and deep learning methods for Internet of Things (IoT) security," *IEEE Commun. Surv. Tut.*, vol. 22, no. 3, pp. 1646–1685, Third Quarter 2020.

[40] Z. Zhang, Y. Lu, Y. Huang, and P. Zhang, "Neural network-based relay selection in two-way SWIPT-Enabled cognitive radio networks," *IEEE Trans. Veh. Technol.*, vol. 69, no. 6, pp. 6264–6274, Jun. 2020.

[41] X. Wang, "Decision-tree-Based relay selection in dualhop wireless communications," *IEEE Trans. Veh. Technol.*, vol. 68, no. 6, pp. 6212–6216, Jun. 2019.

[42] S.-M. Tseng, Y.-F. Chen, C.-S. Tsai, and W.-D. Tsai, "Deep-learning-Aided cross-layer resource allocation of OFDMA/NOMA video communication systems," *IEEE Access*, vol. 7, pp. 157730–157740, 2019.

[43] S.-M. Tseng, C.-S. Tsai, and C.-Y. Yu, "Outage-capacity-Based cross layer resource management for downlink NOMA-OFDMA video communications: Non-deep learning and deep learning approaches," *IEEE Access*, vol. 8, pp. 140097–140107, 2020.

[44] N. Ye, X. Li, H. Yu, A. Wang, W. Liu, and X. Hou, "Deep learning aided grant-free NOMA toward reliable low-latency access in tactile Internet of Things," *IEEE Trans. Ind. Inform.*, vol. 15, no. 5, pp. 2995–3005, May 2019.

[45] F. Khalid and S. Jangsher, "Upper bound of capacity for a MU-MIMO NOMA in a two way relaying network," in *Proc. 6th Int. Conf. Wireless Netw. Mobile Commun.*, 2018, pp. 1–6.

[46] B. Zheng et al., "Secure NOMA based two-way relay networks using artificial noise and full duplex," *IEEE J. Sel. Areas Commun.*, vol. 36, no. 7, pp. 1426–1440, Jul. 2018.

[47] X. Yue, Y. Liu, S. Kang, A. Nallanathan, and Y. Chen, "Modeling and analysis of two-way relay non-orthogonal multiple access systems," *IEEE Trans. Commun.*, vol. 66, no. 9, pp. 3784–3796, Sep. 2018.

[48] T.-V. Nguyen, T.-N. Tran, K. Shim, T. Huynh-The, and B. An, "A deep-neural-network-based relay selection scheme in wireless-powered cognitive IoT networks," *IEEE Internet Things J.*, vol. 8, no. 9, pp. 7423–7436, May 2021.

[49] J. Park and I. W. Sandberg, "Universal approximation using radial-basis-function networks," *Neural Comput.*, vol. 3, no. 2, pp. 246–257, 1991.

[50] T.-H. Vu, T.-V. Nguyen, D. B. da Costa, and S. Kim, "Performance analysis and deep learning design of underlay cognitive noma-based CDRT networks with imperfect SIC and co-channel interference," *IEEE Trans. Commun.*, vol. 69, no. 12, pp. 8159–8174, Dec. 2021.

[51] S. Bi, C. K. Ho, and R. Zhang, "Wireless powered communication: Opportunities and challenges," *IEEE Commun. Mag.*, vol. 53, no. 4, pp. 117–125, Apr. 2015.

[52] X. Wang, M. Jia, I. W.-H Ho, Q. Guo, and F. C. Lau, "Exploiting full-duplex two-way relay cooperative non-orthogonal multiple access," *IEEE Trans. Commun.*, vol. 67, no. 4, pp. 2716–2729, Apr. 2019.

[53] M. Xia and S. Aissa, "Impact of co-channel interference on the performance of multi-hop relaying over Nakagami-m fading channels," *IEEE Wireless Commun. Lett.*, vol. 3, no. 2, pp. 133–136, Apr. 2014.

[54] A. Goldsmith, *Wireless Communications*. Cambridge, U.K.: Cambridge Univ. Press, 2005.

[55] Z. Yu, C. Zhai, J. Liu, and H. Xu, "Cooperative relaying based non-orthogonal multiple access (NOMA) with relay selection," *IEEE Trans. Veh. Technol.*, vol. 67, no. 12, pp. 11606–11618, Dec. 2018.

[56] D.-T. Do, A.-T. Le, and B. M. Lee, “NOMA in cooperative underlay cognitive radio networks under imperfect SIC,” *IEEE Access*, vol. 8, pp. 86180–86195, 2020.

[57] A. Jeffrey and D. Zwillinger, *Table of Integrals, Series, and Products*. Amsterdam, The Netherlands: Elsevier, 2007.

[58] K. P. Peppas, “A new formula for the average bit error probability of dual-hop amplify-and-forward relaying systems over generalized shadowed fading channels,” *IEEE Wireless Commun. Lett.*, vol. 1, no. 2, pp. 85–88, Apr. 2012.

[59] H. Lei, I. S. Ansari, G. Pan, B. Alomair, and M.-S. Alouini, “Secrecy capacity analysis over - fading channels,” *IEEE Commun. Lett.*, vol. 21, no. 6, pp. 1445–1448, Jun. 2017.

[60] A. M. Mathai, R. K. Saxena, and H. J. Haubold, *The H-Function: Theory and Applications*. Berlin, Germany: Springer Science & Business Media, 2009.

[61] X. Li, J. Li, Y. Liu, Z. Ding, and A. Nallanathan, “Residual transceiver hardware impairments on cooperative NOMA networks,” *IEEE Trans. Wireless Commun.*, vol. 19, no. 1, pp. 680–695, Jan. 2020.

[62] Y.-C. Chang, “N-dimension golden section search: Its variants and limitations,” in *Proc. 2nd Int. Conf. Biomed. Eng. Inform.*, 2009, pp. 1–6.

[63] K. Shim, T.-V. Nguyen, and B. An, “Exploiting opportunistic scheduling schemes to improve physical-layer security in MU-MISO NOMA systems,” *IEEE Access*, vol. 7, pp. 180867–180886, 2019.

[64] H. Lu, Y. Zeng, S. Jin, and R. Zhang, “Aerial intelligent reflecting surface: Joint placement and passive beamforming design with 3D beam flattening,” *IEEE Trans. Wireless Commun.*, vol. 20, no. 7, pp. 4128–4143, Jul. 2021.

[65] T. N. Do, G. Kaddoum, T. L. Nguyen, D. B. Da Costa, and Z. J. Haas, “Aerial reconfigurable intelligent surface-aided wireless communication systems,” in *Proc. IEEE 32nd Annu. Int. Symp. Pers., Indoor Mobile Radio Commun.*, 2021, pp. 525–530.

[66] Y. Cheng, K. H. Li, Y. Liu, K. C. Teh, and H. V. Poor, “Downlink and uplink intelligent reflecting surface aided networks: NOMA and OMA,” *IEEE Trans. Wireless Commun.*, vol. 20, no. 6, pp. 3988–4000, Jun. 2021.

[67] V. Adamchik and O. Marichev, “The algorithm for calculating integrals of hypergeometric type functions and its realization in REDUCE system,” in *Proc. Int. Symp. Symbolic Algebr. Comput.*, 1990, pp. 212–224.

[68] A. Prudnikov, Y. Brychkov, I. Brychkov, and O. Marichev, *Integrals and Series. Volume 3: More Special Functions*. London, U.K.: Gordon and Breach Science Publishers, 1986. [Online]. Available: https://books.google.com.vn/books?id=OdS6QgAACAAJ

[69] M. D. Springer, *The Algebra of Random Variables*. Hoboken, NJ, USA: Wiley, 1979.

[70] P. Mittal and K. Gupta, “An integral involving generalized function of two variables,” *Proc. Indian Acad. Sci.–Section A*, vol. 75, no. 3, pp. 117–123, 1972.

[71] M. Abramowitz, I. A. Stegun, and R. H. Romer, “Handbook of Mathematical Functions With Formulas, Graphs, and Mathematical Tables,” 1988.

Anh-Tu Le (Member, IEEE) received the BS degree from the Industrial University of Ho Chi Minh City, Vietnam, in 2019, and the MS degree from Ton Duc Thang University, Vietnam, in 2022. He has authored and co-authored more than 25 ISI-indexed journals. His research interests include wireless channel modeling, NOMA, cognitive radio, MIMO, and machine learning.

Dinh-Hieu Tran (Student Member, IEEE) received the MSc degree in electronics and computer engineering from Hongik University, Korea, in 2017, and the PhD degree from the University of Luxembourg, in 2022, under the supervision of Prof. Symeon Chatzinotas and Prof. Björn Ottersten. He is currently a senior research specialist 5G+ with Nokia Bell Labs, France. His major interests include non-terrestrial-network, 5G+ for wireless communication networks. In 2016, he received the Hongik Rector Award during his master’s study with Hongik University. He was a co-recipient of the IS3C 2016 best paper award. In 2022, he was nominated for the “FNR Outstanding Thesis Award” and won the award “Excellent thesis award 2022 in Doctoral School Science and Engineering.

Chi-Bao Le is currently working toward the master’s degree in wireless communications. He is currently a frontend developer with Transcosmos Vietnam Company, Ltd., Vietnam. He has published more than 45 SCI/SCIE journal articles, three conference papers, and three book chapters. His research interests include signal processing in wireless communications networks, non-orthogonal multiple access, backscatter, reconfigurable intelligent surfaces, and physical-layer security.

Phu Tran Tin received the bachelor’s degree from the Ho Chi Minh City University of Science, in 2002, and the master’s degree from Ho Chi Minh City, Vietnam, in 2008, and the PhD degree from the Faculty of Electrical Engineering and Computer Science, VSB–Technical University of Ostrava, Ostrava, Czechia, in 2019. He is currently a lecturer with the Faculty of Electronics Technology, Industrial University of Ho Chi Minh City, Ho Chi Minh City. His major research interests are wireless communication in 5G, energy harvesting, performance of cognitive radio, physical-layer security, and NOMA.

Tan N. Nguyen (Member, IEEE) received the BS degree in electronics from the Ho Chi Minh University of Natural Sciences, in 2008, the MS degree in telecommunications engineering from Vietnam National University, in 2012, and the PhD degree in communications technologies from the Faculty of Electrical Engineering and Computer Science, VSB – Technical University of Ostrava, Czech Republic, in 2019. He joined the Faculty of Electrical and Electronics Engineering of Ton Duc Thang University, Vietnam, in 2013, and since then has been lecturing. He started as the editor-in-chief of *Advances in Electrical and Electronic Engineering (AEEE)* journal, in 2023. His major interests are cooperative communications, cognitive radio, signal processing, satellite communication, UAV, and physical layer security.

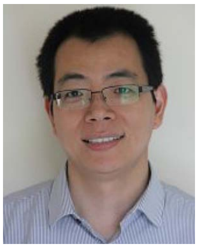

Zhiguo Ding (Fellow, IEEE) received the BEng degree in electrical engineering from the Beijing University of Posts and Telecommunications, in 2000, and the PhD degree in electrical engineering from Imperial College London, in 2005. He is currently a professor of communications with Khalifa University. Previously, he worked with Queen's University Belfast, Imperial College London, Newcastle University, and Lancaster University. From 2012 to 2023, he has also been an academic visitor with the Prof. Vincent Poor's Group, Princeton University. His research interests include B5G networks, machine learning, cooperative and energy harvesting networks, and statistical signal processing. He is a member of the Global Research Advisory Board of Yonsei University. He recently received the EU Marie Curie Fellowship from 2012 to 2014, the Top *IEEE Transactions on Vehicular Technology* editor, in 2017, the IEEE Heinrich Hertz Award, in 2018, the IEEE Jack Neubauer Memorial Award, in 2018, the IEEE Best Signal Processing Letter Award, in 2018, the Friedrich Wilhelm Bessel Research Award, in 2020, and the Best Paper Award at IEEE ICCC-2021. He is serving as an area editor for the *IEEE Open Journal of the Communications Society* and an editor for *IEEE Transactions on Wireless Communications*, *IEEE Transactions on Vehicular Technology*, and *IEEE Communications Surveys and Tutorials*. He was an editor of *IEEE Wireless Communication Letters*, *IEEE Transactions on Communications*, and *IEEE Communication Letters*, from 2013 to 2016. He is a Web of Science Highly Cited Researcher in two disciplines (2019–2023). He is an IEEE ComSoc distinguished lecturer.

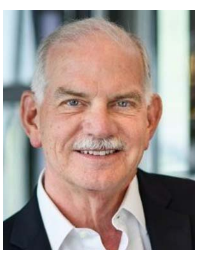

H. Vincent Poor (Life Fellow, IEEE) received the PhD degree in EECS from Princeton University, in 1977. From 1977 to 1990, he was on the faculty of the University of Illinois at Urbana-Champaign. Since 1990 he has been on the faculty with Princeton, where he is currently the Michael Henry Strater University professor. During 2006 to 2016, he served as the dean of Princeton's School of Engineering and Applied Science. He has also held visiting appointments with several other universities, including most recently with Berkeley and Cambridge. His research interests are in the areas of information theory, machine learning and network science, and their applications in wireless networks, energy systems, and related fields. Among his publications in these areas is the recent book Machine Learning and Wireless Communications. (Cambridge University Press, 2022). He is a member of the National Academy of Engineering and the National Academy of Sciences and is a foreign member of the Chinese Academy of Sciences, the Royal Society, and other national and international academies. He received the IEEE Alexander Graham Bell Medal, in 2017.

Miroslav Voznak (Senior Member, IEEE) received the PhD degree in telecommunications from the Faculty of Electrical Engineering and Computer Science, VSB–Technical University of Ostrava, and the Habilitation degree, in 2009. He was appointed as a full professor of electronics and communications technologies, in 2017. He is a Principal Investigator in the research project QUANTUM5 funded by NATO, which focuses on the application of quantum cryptography in 5G campus networks. He participated in six projects funded by the EU in programs managed directly by European Commission. He has authored and coauthored more than more than one hundred scientific articles in SCI/SCIE journals. His research interests include generally ICT, especially quality of service and experience, network security, wireless networks, and Big Data analytics. Since 2020 he has been ranked among the World's Top 2% Scientists by Stanford University in the subfield Networking & Telecommunications. He served as the general chair for the 11th IFIP Wireless and Mobile Networking Conference, in 2018, and for the 24th IEEE/ACM International Symposium on Distributed Simulation and Real Time Applications, in 2020.